

# Giant momentum-dependent spin splitting in symmetric low Z antiferromagnets

Lin-Ding Yuan<sup>1</sup>, Zhi Wang<sup>1\*</sup>, Jun-Wei Luo<sup>2</sup>, Emmanuel I. Rashba<sup>3\*</sup>, Alex Zunger<sup>1\*</sup>

The energy vs. crystal momentum  $E(k)$  diagram for a solid ('band structure') constitutes the road map for navigating its optical, thermodynamic and transport properties. By selecting crystals with specific atom types, composition and symmetries one could design a target band structure and thus desired properties. A particularly attractive outcome would be to design energy bands that are split into spin components with a momentum-dependent splitting, enabling spintronic application. The current paper provides theoretical evidence for wavevector dependent spin splitting of energy bands<sup>1</sup> that parallels the traditional Dresselhaus<sup>2</sup> and Rashba<sup>3</sup> spin-orbit coupling (SOC) -induced splitting, but originates from a fundamentally different source — antiferromagnetism. Identifying via theoretically derived design principles a compound (tetragonal  $\text{MnF}_2$ ) with the right magnetic symmetry and performing density functional band structure calculations, reveals surprising, hitherto unknown spin behaviors. Unlike the traditional SOC-induced effects<sup>2,3</sup> restricted to non-centrosymmetric crystals, we show that antiferromagnetic-induced spin splitting broadens the playing field to include even centrosymmetric compounds, and is nonzero even without SOC, and consequently does not rely on the often-unstable high atomic number elements required for high SOC, and yet is comparable in magnitude to the best known ('giant') SOC effects. This work identifies predicted fingerprints of the novel spin splitting mechanism to aid its eventual experimental measurements. It envisions that the antiferromagnetic induced spin-split energy bands would be beneficial for efficient spin-charge conversion and spin orbit torque applications without the burden of requiring compounds containing heavy elements.

---

Corresponding authors: Alex Zunger, Zhi Wang

<sup>1</sup>*Energy Institute, University of Colorado, Boulder, CO 80309, USA*

<sup>2</sup>*State Key Laboratory for Superlattices and Microstructures, Institute of Semiconductors, Chinese Academy of Sciences, Beijing 100083, China.*

<sup>3</sup>*Department of Physics Harvard University, Cambridge, Massachusetts 02138, USA*

Emails: [erashba@physics.harvard.edu](mailto:erashba@physics.harvard.edu) ; [alex.zunger@colorado.edu](mailto:alex.zunger@colorado.edu)

An electron with momentum  $\mathbf{p}$  and mass  $m$  moving in an inversion symmetry-breaking electric field  $\mathbf{E}$  in a solid experiences an effective magnetic field  $\mathbf{B}_{\text{eff}} \sim \mathbf{E} \times \mathbf{p}/mc^2$  in its rest-frame, where  $c$  is the speed of light. In bulk crystals<sup>2</sup> this symmetry breaking electric field is given by the gradient of the crystal potential  $\mathbf{E} = -\nabla V$ , whereas in heterostructures<sup>3</sup> it can be produced by interfacial asymmetry, and in centrosymmetric compounds by the local asymmetry of individual structural sectors<sup>4</sup>. This intrinsic magnetic field couples the electron momentum to its spin, a relativistic effect leading to spin-orbit-coupling (SOC) induced spin splitting of energy bands at wave vectors differing from the time reversal invariant moments (TRIM). In the semi-relativistic Pauli equation, the SOC is described by the Thomas<sup>5</sup> term  $H_T = -\frac{e\hbar}{4m^2c^2}[\boldsymbol{\sigma} \cdot (\nabla V(\mathbf{r}) \times \mathbf{p})]$ , that couples electron spin  $\boldsymbol{\sigma}$  to its coordinate  $\mathbf{r}$  and momentum  $\mathbf{p}$ , and its fully relativistic generalization. These seminal studies have formed the basis for the development of spintronics<sup>6-8</sup>, bringing  $\mathbf{k}$ -dependent spin-orbit interaction to the forefront of solid-state physics, including applications to spin transistor, spin-orbit torque, spin Hall effect, topological insulators, and Majorana Fermions (see review in Ref. <sup>9</sup>). Since the relativistic spin-orbit interaction increases rapidly with atomic number  $Z$ , and since the strength of chemical bonds in compounds decreases rapidly with increasing atomic number<sup>10</sup>, the ease of breaking such fragile bonds-- creating free-carrier generating metal vacancies-- has been an unwelcome but constant companion of high SOC compounds both for spin splitting and for topological insulators applications.<sup>11-14</sup> This double limitation to high- $Z$  and non-centrosymmetric compounds has raised hopes for an alternative spin splitting mechanism in thermodynamically stable, low  $Z$  compounds of more general symmetries.

More recently, the investigation of spin splitting of energy bands has been expanded to include in addition to non-magnetic (NM)<sup>15</sup> and ferromagnetic (FM) systems, also antiferromagnetic (AFM) ones, in particular for eliminating stray fields around FM elements.<sup>16-19</sup> It is generally implied that such SOC-induced splitting in the presence of background AFM may be treated just as SOC in NM materials, through the same Thomas term<sup>5</sup>. Indeed, BiCoO<sub>3</sub><sup>20</sup> manifests a small change in spin splitting due to its antiferromagnetism, and, as shown in Ref. <sup>20</sup>, if SOC is deliberately removed from the Hamiltonian, the system has zero spin splitting in the whole Brillouin Zone (BZ). Here we uncover a different AFM effect whereby spin splitting exists even in centrosymmetric crystals, and even if SOC is deliberately removed from the Hamiltonian (i.e., in low  $Z$  compounds), and persists at time reversal invariant wave vectors. The field-free magnetic mechanism discussed in the present paper differs also from the anomalous spin-orbit coupling in antiferromagnets induced by applying external magnetic field, discussed in Ref. <sup>21,22</sup>.

A phenomenological theory of magnetic spin splitting has been proposed 1964 by Pekar and Rashba<sup>1</sup>, suggesting that the presence in magnetic compounds of a spatially inhomogeneous intrinsic magnetic field  $\mathbf{h}(\mathbf{r})$ , periodic with the crystal period, can lead to coupling of Pauli matrices  $\boldsymbol{\sigma}$  to this  $\mathbf{h}(\mathbf{r})$ , resulting in a magnetic mechanism of  $\mathbf{k}$ -dependent spin splitting. In terms of the relativistic expansion in  $1/c$ , this magnetic mechanism is of the same order  $1/c^2$  as the Thomas term because both the Bohr magneton  $\mu_B = e\hbar/2mc$  and the field  $\mathbf{h}(\mathbf{r})$  produced by electron magnetization are of the order of  $1/c$ . Because the  $\mathbf{k} \cdot \mathbf{p}$  formalism used in Ref. <sup>1</sup> did not afford an atomistic definition of  $\mathbf{h}(\mathbf{r})$  and its ensuing spin splitting, nor did it provide for guiding principles to select a target material for investigating such effects, examination of these 1964 ideas<sup>1</sup> remained dormant for a long time.

To select a compound for direct magnetic  $\mathbf{k}$ -dependent spin splitting we inspect the underlying symmetry requirements ('design principles'). Since in non-magnetic materials the combined symmetry of time reversal  $\theta$  and spatial inversion  $I$  ensures double degeneracy for arbitrary wave vector  $\mathbf{k}$ , the appearance of spin splitting requires violation of  $\theta I$  symmetry. To break  $\theta I$  in NM cases it is enough to violate the inversion symmetry  $I$ , i.e., to consider non-centrosymmetric structures. However, in magnetic crystals, where  $\theta$  is already violated due to magnetic order, absence of  $I$  symmetry is neither necessary nor sufficient condition of breaking of  $\theta I$ , hence does not necessarily lead to the removal of spin degeneracy. Actually, even for a *centrosymmetric* magnetic structure, where  $I$  is preserved but  $\theta I$  is broken, one can still have  $\mathbf{k}$ -dependent spin splitting contributed by both SOC mechanism and magnetic mechanism. We note that depending on the existence or absence of additional symmetries, one can have additional types of AFM-induced spin splitting, e.g., not necessarily centrosymmetric (see supplementary I). Since the existence of  $\mathbf{k}$ -dependent spin splitting even in centrosymmetric crystals is one of the most significant differences between the SOC mechanism and the magnetic mechanism, we proceed here with the above noted 'design principles', namely focus on AFM insulating and centrosymmetric compound that violates  $\theta I$  symmetry.

To this end, we search the Bilbao listing<sup>23</sup> of symmetry of magnetic compounds, select AFM tetragonal  $\text{MnF}_2$  having magnetic space group  $P4_2'/\text{mnm}'$  as complying with the above noted symmetries.  $\text{MnF}_2$  is a wide gap insulator both below and above its Néel temperature of 67K.<sup>24</sup> It is a centrosymmetric rutile structure (space group  $P4_2/\text{mnm}$ ), with magnetic Mn ions occupying position (0, 0, 0) and (1/2, 1/2, 1/2) centered in an octahedral of non-magnetic F anions located at  $\pm(u, u, 0)$  and  $\pm(1/2+u, 1/2-u, 1/2)$  where  $u$  is the positional parameter. The refinement X-ray diffraction results<sup>25</sup> gave the positional parameter  $u=0.305$ , and lattice constant  $a=b=4.873 \text{ \AA}$ ,  $c=3.311 \text{ \AA}$ . Erickson<sup>26</sup> found via neutron scattering measurements the AFM moment aligned along the tetragonal axis (i.e., [001]) with magnetic space group of  $P4_2'/\text{mnm}'$ . The magnetic crystal unit cell is shown in Figure 1(a).

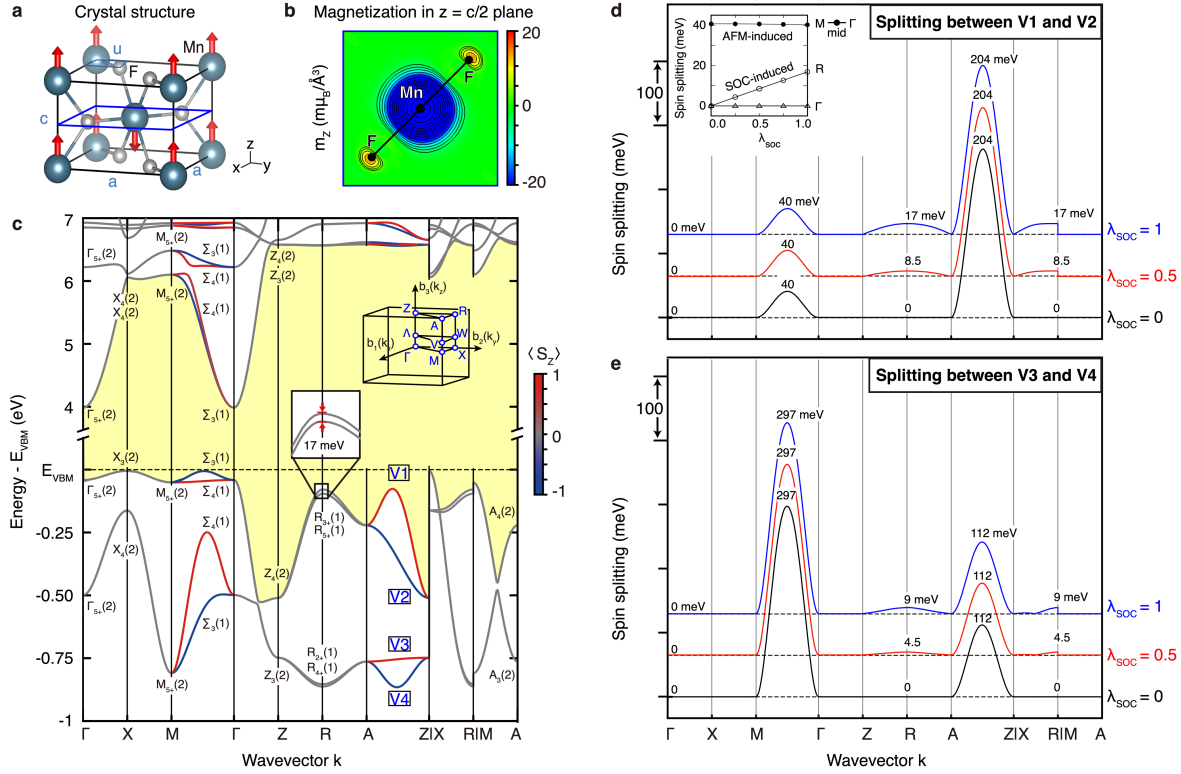


**Figure 1 | Crystal structure, band structure and spin splitting in centrosymmetric AFM tetragonal  $\text{MnF}_2$ .** (a) Magnetic unit cell where red arrows indicate local magnetic moment; (b) contour plot of magnetization along  $z$  in  $z = c/2$  plane; (c) DFT calculated band structure with our calculated magnetic symmetry representations (see supplementary section II), using the notations of Ref. <sup>27</sup> with numbers in parenthesis indicating the dimension of the representation (i.e., degeneracies). The top four valence bands are denoted by V1, V2, V3, V4 and the yellow screen highlights the gaps between valence and conduction bands. Insert of (c) shows the BZ and the blow-up bands around R point. The blue to red color scale denotes calculated out-of-plane spin polarization. Panels (d, e) show DFT calculated wave vector dependence of the spin splitting between pairs of valence bands V1-V2 (in (d)) and between V3-V4 (in (e)) for different scaling of SOC  $\lambda_{\text{SOC}}$  (numerical coefficient  $0 < \lambda_{\text{SOC}} < 1$ ). Insert of (d) shows the spin splitting vs. the amplitude of the spin orbit coupling  $\lambda_{\text{SOC}}$  at  $\Gamma$  (0, 0, 0), R (0, 0.5, 0.5) and the middle point of  $\Gamma$ -M (0.25, 0.25, 0). All DFT calculations use PBE exchange correlation functional<sup>28</sup> with on-site coulomb interaction on Mn-3d orbitals of  $U = 5\text{ eV}$ ,  $J = 0\text{ eV}$  and the experimental crystal structure<sup>25</sup>.

We calculate the relativistic electronic structure of AFM  $\text{MnF}_2$  within density functional theory (DFT) (see description of DFT method in supplementary section II). Fig 1(b) provides the calculated magnetization  $m_z(\mathbf{r}) = m^\uparrow(\mathbf{r}) - m^\downarrow(\mathbf{r})$  in the  $c=z/2$  plane, with  $m^\uparrow$  and  $m^\downarrow(\mathbf{r})$  representing the up and down spin electron density. Our DFT calculation uses a modality that allows us not only to isolate the spin splitting of the experimental structure (having both AFM and SOC terms), but also to perform self-consistent constrained calculations, where we solve the DFT equations for different SOC strengths (including zero) of AFM phase. The tuning of SOC strength is done by adjusting the coefficient  $\lambda_{\text{SOC}}$  of the SOC term  $\hat{H}_{\text{SOC}} = \lambda_{\text{SOC}} \hat{\mathbf{L}} \cdot \hat{\mathbf{S}}$  in the DFT formalism<sup>29</sup> To assess the AFM magnetism effect we also define a reference NM model, where the magnetic moment on each site is zero, resulting in a metallic state. We emphasize that the NM model is not used to mimic the physical high temperature

paramagnetic phase that has a distribution of non-vanishing local magnetic moments that creates an insulating gap even in the absence of long-range order.<sup>30,31</sup> Figure 1(c) gives the band structure of the AFM phase calculated with SOC in its experimental crystal structure. We find a z oriented magnetic moment on  $\text{Mn}^{2+}$  of  $4.7 \mu_B$ , in good agreement with the neutron scattering measurement of  $4.6 \mu_B$ . We also find calculated minimum direct gap at  $\Gamma$  of 4.02 eV and a smaller indirect gap between VBM at X and CBM at  $\Gamma$  of 3.98 eV, comparable with the measured absorption gap<sup>32</sup> of 4.1 eV (estimated from the convergence limit of the observed series of discrete d-d\* multiplet transitions into the onset of band-to-band continuum).

To assist future measurements of the predicted AFM-induced  $\mathbf{k}$ -dependent spin splitting (e.g. via ARPES and spin-ARPES) as well as potential applications in novel spintronics we next describe the main predicted features of the AFM-induced spin splitting.

(i) The splitting has a typical atomic energy scale (“giant splitting”): Despite rather small atomic numbers in  $\text{MnF}_2$  ( $Z(\text{Mn})= 25$  and  $Z(\text{F})= 9$ ), the magnitude of the spin splitting (up to 300 meV seen between V3 and V4 along  $\Gamma$ -M in Figure 1(e)) arising from the AFM mechanism can be comparable to some of the largest known spin splitting of conventional electric mechanism for heavy atom high Z compounds, such as the ‘giant SOC’ induced spin splitting in  $\text{BiTeI}$ <sup>33</sup> and  $\text{GeTe}$ <sup>34,35</sup>. The reason for the difference is that the magnetic field which induces the splitting in AFM reflects the local magnetic moments localized about atomic sites, not as in the SOC effect where the inducing magnetic field reflects the asymmetry in the inter-atomic regions of the unit cell.

(ii) The splitting persists even if SOC= 0: The spin splitting along the  $\Gamma$ -M and Z-A lines is present even when SOC is turned off in the Hamiltonian (black line in Figure 1(d) and (e); also shown in the insert of (d)). This is very different from the case of spin splitting found in AFM  $\text{BiCoO}_3$ <sup>20</sup>, where spin splitting disappears if SOC vanishes. Such momentum dependent but SOC unrelated spin splitting has also been reported recently based on tight-binding model<sup>36</sup> from which the authors derive symmetry invariant spin splitting terms. Thus, the AFM-induced spin splitting mechanism described here delivers the long-standing hope for wave vector dependent spin splitting mechanism in thermodynamically stable, low Z compounds.

(iii) Relative to the NM case, AFM induces a highly anisotropic and  $\mathbf{k}$ -dependent spin splitting: We show in Figure 2 the band structures of centrosymmetric  $\text{MnF}_2$  in two cases (a) NM without SOC; (b) AFM without SOC. In both cases we indicate the degeneracies of states, calculated by DFT shown as integer values. In this description the NM model (where spin up and spin down have the same energy) is metallic because the five d electrons of  $\text{Mn}^{2+}$  occupy only partially the six degenerate crystal field  $t_{2g}$  states. Going from the NM model to the AFM phase, local moments are allowed to develop and spin up states acquire different energy relative to spin down. This exchange type interaction opens an insulating gap between spin up and spin down orbitals as the five Mn d electrons occupy a complete shell configuration of  $t_{2g\uparrow}^3 e_{g\uparrow}^2 t_{2g\downarrow}^0 e_{g\downarrow}^0$ .

An important manifestation of the AFM- induced spin splitting (Figure 1(c)) is that whereas in the NM structure, the whole BZ, including directions  $\Gamma$ -X and  $\Gamma$ -M, have double degenerate non split bands, in

the AFM structure spin splitting arises even in the absence of SOC but it is wave vector dependent: bands remain degenerate along the  $\Gamma$ -X directions, but become spin split along the  $\Gamma$ -M direction. Such anisotropic spin splitting was already hinted by the asymmetric in magnetization in coordinate space as shown in Figure 1(b) between  $x + y$ ,  $x - y$  and  $x$ ,  $y$  directions. This behavior is understandable on the basis of magnetic symmetry (See supplementary III for discussion of unitary and anti unitary symmetries): the AFM ordering does not lead to symmetry reduction along the  $\Gamma$ -X paths, relative to its NM counterpart. The resulting spin degeneracy along  $k_x$  (or  $k_y$ ) direction of  $\Gamma$ -X in AFM is protected by its group of  $\mathbf{k}$  symmetries  $\theta\{C_{2x}|\tau\}$  and  $\theta\{\sigma_{vy}|\tau\}$  (or  $\theta\{C_{2y}|\tau\}$  and  $\theta\{\sigma_{vx}|\tau\}$ ). In contrast, along the  $\Gamma$ -M paths, in AFM the combined symmetries of  $\theta\{C_{2a}|0\}$  and  $\theta\{C_{2b}|0\}$  (or  $\theta\{\sigma_{da}|0\}$  and  $\theta\{\sigma_{db}|0\}$ ) are broken, which creates spin splitting. Here,  $C_{2x}$ ,  $C_{2y}$ ,  $C_{2a}$ ,  $C_{2b}$  are  $\pi$  rotations about the  $[100]$ ,  $[010]$ ,  $[110]$ ,  $[1-10]$  axes, respectively;  $\sigma_{vx}$ ,  $\sigma_{vy}$ ,  $\sigma_{da}$ ,  $\sigma_{db}$  are mirror reflections in  $(100)$ ,  $(010)$ ,  $(1-10)$ ,  $(110)$  planes; and vector  $\tau = (1/2, 1/2, 1/2)$  is half lattice translation, directed along the spatial diagonal  $[111]$  of the unit cell. Similar arguments (given in Supplementary section III) apply for spin degeneracy along Z-R and spin splitting along Z-A in Figure 1(b).

(iv) The AFM mechanism gives rise to even powers of  $k$  in the spin splitting near degeneracy points compared with odd powers typical of the electrically-induced effect. Of special interest in Figure 1 (c) is the diagonal  $\Gamma$ -M and Z-A line in the base  $k_z = 0$  plane of BZ, showing large spin splitting while at the end of these  $k$ -lines the splitting vanishes. It is of interest therefore, to establish how the splitting changes near its end points. By fitting the DFT calculated spin splitting  $\Delta_{ss}(\mathbf{k})$  to the power of  $k$ , we found a quadratic-in- $k$  dependence at  $\Gamma_{\Gamma-M}$  and  $M_{M-\Gamma}$  (see details of fitting in supplementary VI). These remarkable features of the spin splitting around  $\Gamma$  and Z can be captured via a two-band effective spin split model  $H = \sigma_z k_x k_y$  (invariant term second order in  $\mathbf{k}$ ), which gives rise to two spin split bands with energy  $E_{\pm} = \pm k_x k_y$ . (See derivation of the AFM effective model at  $\Gamma$  and Z for the presence or absence of SOC in Supplementary section V). Such analytic, symmetry determined effective Hamiltonians are then fit to DFT (rather than attempting a KP solution) to establish the pertinent realistic energy scale. This proves that the spin splitting  $\Delta_{ss}(\mathbf{k}) = E_+ - E_-$  has a  $k^2$  dependence along the diagonal  $k_x = k_y$  directions of  $\Gamma$ -M and Z-A, as found by direct DFT calculations.

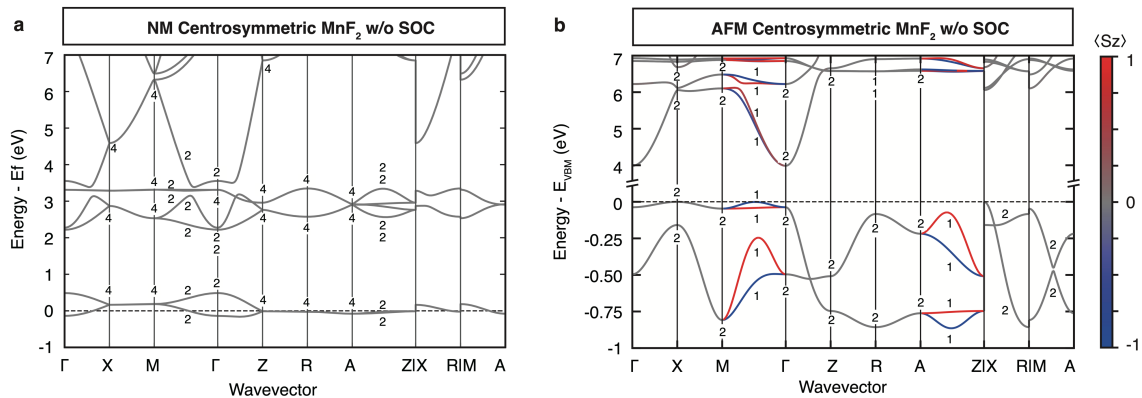


**Figure 2 | DFT band structures of Centrosymmetric (CS) MnF<sub>2</sub> in NM and AFM without SOC.** In all cases we use the experimentally observed centrosymmetric tetragonal structure<sup>25</sup>: (a) NM with SOC set to

zero; **(b)** AFM with SOC set to zero. Out-of-plane spin polarizations are mapped to color scales from blue to red. The integer number attached to each band and  $\mathbf{k}$  point is degeneracies.

(v) A Dresselhaus in-plane spin texture results from a cooperative SOC and AFM effect: The coupling between spin space and position space results not only in spin-splitting of the energy spectrum, but also in developing “spin-momentum locking” where the spin orientation is locked with momentum  $\mathbf{k}$ . The vector field of the spin states in momentum space is called spin texture, being helical for the conventional Rashba SOC mechanism<sup>3</sup> and non-helical for the Dresselhaus mechanism<sup>2</sup>. The spin texture for AFM-induced spin splitting has its own fingerprints. Figure 3 shows the calculated spin texture of the V1 and V2 bands at the representative  $\mathbf{k}$ -plane  $k_z = \pi/2c$  where  $c$  is the lattice constant along  $z$  axis. We see that, electron spins are mostly aligned along the out-of-plane  $z$  direction, as can be surmised from the magnetic structure (see Figure 1(a)). This is seen in the four quadrants patterns on a fixed  $k_z$  plane with positive (up arrow in Figure 3(a) and (b)) and negative (down arrow in Figure 3(a) and (b)) out-of-plane spin polarization in the neighbor quadrants. The out-of-plane spin polarizations are opposite in sign between bands V1 and V2, as noted by the reversal of the red and blue patterns for V1 and V2. Similar four quadrants pattern of out-of-plane spin polarization is also found in the  $k_z = 0$  and  $k_z = \pi/c$  planes (see corresponding spin texture results in Supplementary section VI). More interestingly, inspecting the  $k_z = \pi/2c$  plane in Figure 3 shows a pronounced *in-plane* non-helical Dresselhaus-like spin texture in the  $z$ -oriented magnetized AFM compound given that the crystal structure is centrosymmetric that normally is required to break to assure Dresselhaus features<sup>4</sup>. We find that this Dresselhaus spin texture seen here requires for its existence the SOC term (it vanishes as the SOC is removed from the Hamiltonian), and thus represents the effect of coexistence of SOC with AFM (see cooperative effect on spin splitting in section VII). Observation of this unusual spin texture is called for.

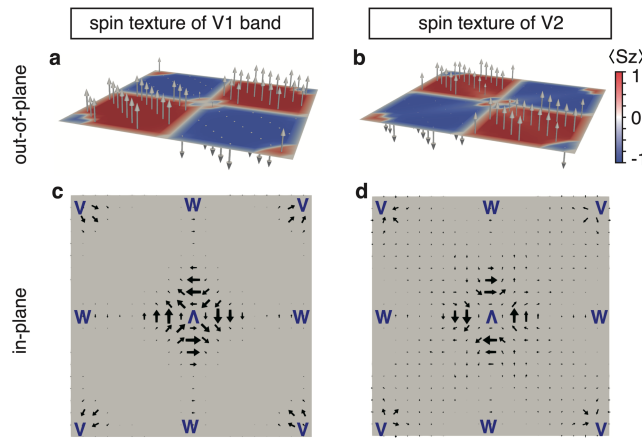


**Figure 3 | Spin texture in AFM  $\text{MnF}_2$  with SOC on  $k_z = \pi/2c$  plane. (a)** Out-of-plane spin texture of V1 band, **(b)** out-of-plane spin texture of V2 band, **(c)** in-plane spin texture of V1 band, and **(d)** in-plane spin texture of V2 band.

(vi) Different wavevectors can have different dependence on SOC: The insert of Figure 1(d) shows different characteristic behaviors of the dependence of spin splitting  $\Delta_{ss}(\mathbf{k})$  on spin-orbit strength at

different  $\mathbf{k}$  points: (1) The trivial case (e.g.  $\Gamma$  point) is that neither magnetic nor SOC induces any splitting; (2) the R point shows zero spin splitting when  $\lambda_{SOC} = 0$  and linear dependence of  $\lambda_{SOC}$ , illustrating a cooperation of both magnetic and SOC mechanism; notice that despite R being a TRIM point, it shows spin splitting, unlike the case of purely SOC induced effects; (3) the non-trivial case of purely magnetic induced spin splitting occurs along  $\Gamma$ -M (as well as A-Z) line, where non-zero spin splitting is present even at  $\lambda_{SOC} = 0$  and is almost independent of  $\lambda_{SOC}$ . The appearance of such distinct spin splitting behaviors at different wave vectors in a single compound would be advocated for multifunctional spintronic applications.

## DISCUSSION

An AFM-induced mechanism of the momentum-dependent spin-splitting of spin energy bands offers important advantages relative to the traditional electric mechanism of spin splitting<sup>2,3</sup> that relies on high SOC compounds made of heavy elements, some of them prone to structural defects. The two main observations are (i) giant magnitude of spin splitting, of potential critical importance for applications, and (ii) developing spectacular difference between  $(x, y)$  and  $(x + y, x - y)$  axes that are equivalent in non-magnetic case but becomes drastically nonequivalent in AFM phase. The role of the dynamic internal magnetic field in the traditional SOC spin splitting<sup>2,3</sup> (induced by electron movement in an electric field) is replaced in AFM compounds by the static magnetic field which does not vanish even if SOC=0, and couples the spin with the magnetic order to the wave vector  $\mathbf{k}$ . This study uncovers a very rich set of fingerprint fundamental physical effects [(i)-(vi) above], primarily the giant spin splitting that characterizes the AFM mechanism and could aid its experimental observation as well as potential exploratory applications in novel spintronics. The present symmetry-based theory with atomistic resolution enabled by DFT instills content into the 1964 phenomenological theory by Pekar and Rashba<sup>1</sup> proposing a pioneering magnetic spin splitting mechanism.

**Data availability.** The data that support the findings of this study are available from the corresponding author upon reasonable request.

**Acknowledgment.** The National Science Foundation (NSF) Grant NSF-DMR-CMMT No DMR-1724791 supported the theory development of this work by L.-D.Y., Z.W., and A.Z. at the University of Colorado Boulder. The *ab initio* calculations of this work were supported by the U.S. Department of Energy, Office of Science, Basic Energy Sciences, Materials Sciences and Engineering Division under Grant No. DE-SC0010467. J.-W. L. was supported by the National Natural Science Foundation of China (NSFC) under Grant Number 61888102. This work used resources of the National Energy Research Scientific Computing Center, which is supported by the Office of Science of the U.S. Department of Energy under Contract No. DE-AC02-05CH11231. We thank Dr. Carlos Mera Acosta for fruitful discussions.



**Author contribution.** AZ and ER conceived and directed the study. LDY did the majority of the computational work and analysis; ZW participated in the computation and numerical method development; JWL contributed to the writing and discussions; AZ directed the analysis and wrote the text with input from all authors.

**Competing interests.** The authors declare no competing interests.

**Correspondence and requests for materials** should be addressed to A.Z.

## REFERENCES

1. Pekar, S. & Rashba, E. Combined resonance in crystals in inhomogeneous magnetic fields. *Zh. Eksperim. i Teor. Fiz.* **47**, 1927-1932 (1964): English translation: *Sov. Phys. - JETP* **20**, 1295 (1965)
2. Dresselhaus, G. Spin-Orbit Coupling Effects in Zinc Blende Structures. *Phys Rev* **100**, 580–586 (1955).
3. Rashba, E. & Sheka, V. Symmetry of energy bands in crystals of wurtzite type II. Symmetry of bands with spin-orbit interaction included. *Fiz. Tverd. Tela, Collected Papers (Leningrad)*, v. 2, 162 (1959) (in Russian), English translation:  
[http://iopscience.iop.org/13672630/17/5/050202/media/njp050202\\_suppdata.pdf](http://iopscience.iop.org/13672630/17/5/050202/media/njp050202_suppdata.pdf)
4. Zhang, X., Liu, Q., Luo, J.-W., Freeman, A. J. & Zunger, A. Hidden spin polarization in inversion-symmetric bulk crystals. *Nat Phys* **10**, 387–393 (2014).
5. Landau, L. *et al.* Electrodynamics of continuous media. **8**, (1989) (Oxford, Butterworth-Heinemann), 1989, Sec. 33.
6. Wolf, S. *et al.* Spintronics: A Spin-Based Electronics Vision for the Future. *Science* **294**, 1488–1495 (2001).
7. Žutić, I., Fabian, J. & Sarma, D. S. Spintronics: Fundamentals and applications. *Rev Mod Phys* **76**, 323–410 (2004).
8. Fert, A. The present and the future of spintronics. *Thin Solid Films* **517**, 2–5 (2008).
9. Manchon, A., Koo, H., Nitta, J., Frolov, S. & Duine, R. New perspectives for Rashba spin–orbit coupling. *Nat Mater* **14**, 871–882 (2015).
10. Harrison, W. A. Electronic structure and the properties of solids: the physics of the chemical bond. Courier Corporation, (1989) (table 7-3 and page 176).

11. Taguchi, T. & Ray, B. Point defects in II–VI compounds. *Prog Cryst Growth Charact* **6**, 103–162 (1983).
12. West, D., Sun, Y., Wang, H., Bang, J. & Zhang, S. Native defects in second-generation topological insulators: Effect of spin-orbit interaction on Bi<sub>2</sub>Se<sub>3</sub>. *Phys Rev B* **86**, 121201 (2012).
13. Edwards, A. *et al.* Electronic structure of intrinsic defects in crystalline germanium telluride. *Phys Rev B* **73**, 045210 (2006).
14. Bailly, F. Energies of Formation of Metal Vacancies in II-VI Semiconducting Tellurides (HgTe, CdTe, ZnTe). *Phys Status Solidi B* **25**, 317–322 (1968).
15. Sánchez, R. J. *et al.* Spin-to-charge conversion using Rashba coupling at the interface between non-magnetic materials. *Nature communications* **4**, 2944 (2013).
16. Baltz, V. *et al.* Antiferromagnetic spintronics. *Rev Mod Phys* **90**, 015005 (2018).
17. Jungwirth, T., Marti, X., Wadley, P. & Wunderlich, J. Antiferromagnetic spintronics. *Nat Nanotechnol* **11**, 231–41 (2016).
18. MacDonald, A. & Tsoi, M. Antiferromagnetic metal spintronics. *Philosophical Transactions Royal Soc Math Phys Eng Sci* **369**, 3098–3114 (2011).
19. Manchon, A. *et al.* Current-induced spin-orbit torques in ferromagnetic and antiferromagnetic systems. *Rev Mod Phys* **91**, 035004 (2019).
20. Yamauchi, K., Barone, P. & Picozzi, S. Bulk Rashba Effect in Multiferroics: a theoretical prediction for BiCoO<sub>3</sub>. *arXiv preprint arXiv:1910.06758* (2019).
21. Ramazashvili, R. Kramers Degeneracy in a Magnetic Field and Zeeman Spin-Orbit Coupling in Antiferromagnetic Conductors. *Phys Rev Lett* **101**, 137202 (2008).
22. Rozbicki, E. J., Annett, J. F., Souquet, J.-R. & Mackenzie, A. P. Spin–orbit coupling and k-dependent Zeeman splitting in strontium ruthenate. *Journal of Physics: Condensed Matter* **23**, 094201 (2011).
23. Gallego, S. V. *et al.* MAGNDATA: towards a database of magnetic structures. I. The commensurate case. *J Appl Crystallogr* **49**, 1750–1776 (2016).
24. Stout, J. & Adams, H. Magnetism and the Third Law of Thermodynamics. The Heat Capacity of Manganous Fluoride from 13 to 320°K. *J Am Chem Soc* **64**, 1535–1538 (1942).
25. Baur, W. & Khan, A. Rutile-type compounds. IV. SiO<sub>2</sub>, GeO<sub>2</sub> and a comparison with other rutile-type

structures. *Acta Crystallogr Sect B Struct Crystallogr Cryst Chem* **27**, 2133–2139 (1971).

26. Erickson, R. Neutron Diffraction Studies of Antiferromagnetism in Manganous Fluoride and Some Isomorphous Compounds. *Phys Rev* **90**, 779–785 (1953).

27. Dimmock, J. & Wheeler, R. Symmetry Properties of Wave Functions in Magnetic Crystals. *Phys Rev* **127**, 391–404 (1962).

28. Perdew, J. P. *et al.* Atoms, molecules, solids, and surfaces: Applications of the generalized gradient approximation for exchange and correlation. *Phys Rev B* **46**, 6671–6687 (1992).

29. Steiner, S., Khmelevskiy, S., Marsmann, M. & Kresse, G. Calculation of the magnetic anisotropy with projected-augmented-wave methodology and the case study of disordered Fe  $1 - x$  Co  $x$  alloys. *Phys Rev B* **93**, 224425 (2016).

30. Varignon, J., Bibes, M. & Zunger, A. Origin of band gaps in 3d perovskite oxides. *Nat Commun* **10**, 1658 (2019).

31. Trimarchi, G., Wang, Z. & Zunger, A. Polymorphous band structure model of gapping in the antiferromagnetic and paramagnetic phases of the Mott insulators MnO, FeO, CoO, and NiO. *Phys Rev B* **97**, 035107 (2018).

32. Stout, J. Absorption Spectrum of Manganous Fluoride. *J Chem Phys* **31**, 709–719 (1959).

33. Ishizaka, K. *et al.* Giant Rashba-type spin splitting in bulk BiTeI. *Nat Mater* **10**, 521–526 (2011).

34. Liebmann, M. *et al.* Giant Rashba-Type Spin Splitting in Ferroelectric GeTe(111). *Adv Mater* **28**, 560–565 (2015).

35. Sante, D., Barone, P., Bertacco, R. & Picozzi, S. Electric Control of the Giant Rashba Effect in Bulk GeTe. *Adv Mater* **25**, 509–513 (2012).

36. Hayami, S., Yanagi, Y. & Kusunose, H. Momentum-Dependent Spin Splitting by Collinear Antiferromagnetic Ordering. *J Phys Soc Jpn* **88**, 123702 (2019).